

# An Automated Antenna Measurement System Utilizing Wi-Fi Hardware

Vittorio Picco

IEEE Student Member

Department of Electrical and Computer Engineering

University of Illinois at Chicago, USA

Email: vpicco2@uic.edu

Keith Martin

IEEE Student Member

Department of Electrical and Computer Engineering

University of Illinois at Chicago, USA

Email: kmarti28@uic.edu

**Abstract**—We propose a system that measures 3D gain patterns of an unknown antenna using the Received Signal Strength Indicator (RSSI) provided by Wi-Fi hardware. Our system uses widely available Wi-Fi routers to generate the RF signal and measure incident power. A simple two-axis positioner allows the full 3D pattern of the antenna to be measured, and a LabVIEW interface lets users control measurements and view results. We make use of inexpensive, readily available materials and rudimentary construction techniques.

## I. INTRODUCTION

Measuring the radiation pattern and gain of an antenna is an essential step in assessing compliance with simulation results and design specifications. It is also important for the user that needs to verify the performance of an unknown antenna.

These measurements are typically performed with a network analyzer and an antenna positioner, usually located in an anechoic chamber. A computer synchronizes the movement of the antenna and the network analyzer measurements. As a result, a complete antenna measurement system can cost well over \$100 000, making it an inaccessible commodity for many individuals and institutions. By operating in a limited frequency range and in a non-anechoic environment, it is possible to use widely available components to dramatically decrease the cost of the system. This is accomplished while introducing only minor inaccuracies compared to a typical antenna measurement system.

In this paper we propose an antenna measuring system that makes use of widely available Wi-Fi routers to generate and measure an RF signal at 2.4 GHz. A simple two-axis positioner allows the full 3D pattern of the antenna to be measured, and a LabVIEW interface lets users control measurements and view results. We use inexpensive, readily available materials and rudimentary construction techniques.

## II. THEORY OF ANTENNA MEASUREMENTS

The principles of radiation pattern and gain measurement are well standardized, and rely on the use of at least two antennas. One is referred to as the Measurement Antenna (MA) and the other as the Antenna Under Test (AUT). One works as the transmitter, generating a known field, and the other as the receiver, converting a portion of the incident field into a measurable signal. The reciprocity principle allows either antenna to work as the transmitter or the receiver.

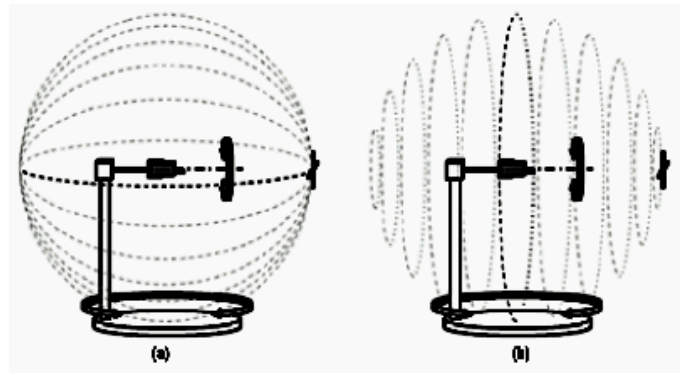


Fig. 1. Two-axis roll-over-yaw positioner realizing great-circle (a) or conical section (b) scans

### A. Pattern measurements

Assuming that the MA is used as the transmitter and the AUT as the receiver, a pattern measurement is obtained by rotating the AUT in front of the MA and recording the incident power received as function of the relative angular position between the two antennas. Full 3D or 2D scans can be achieved depending on the positioner used to rotate the AUT.

We describe the realization of a two axis positioner that allows full 3D pattern measurements. The system allows two axes to be controlled: a lower axis with a vertical axis of rotation – henceforth referred to as the *yaw* axis – and an upper axis with a horizontal axis of rotation – henceforth referred to as the *roll* axis. A schematic representation of the positioner is available in Fig. 1. The imaginary sphere surrounding the antenna can be sampled in different ways using the same positioner structure, depending on how the two axes are controlled. Varying the yaw axis over a constant roll axis position produces great-circle scans; each scan represents a cross-section of the outer sphere, i.e., a circle of maximum diameter. Alternatively, by varying the roll axis for a fixed yaw value, conical section scans are obtained. These represent circles of varying diameter. These circles are the bases of cones of a fixed angle  $\theta$ , the position of the yaw axis. When this method is used, each axis maps directly to the axes of the standard spherical coordinate system. The yaw

axis is equivalent to movement in the  $\theta$  direction, and the roll axis is equivalent to movement in the  $\phi$  direction. To avoid cumbersome coordinate conversions, the conical section method is adopted here.

From this procedure a *relative* pattern measurement is obtained. In order to obtain an absolute measurement of an antenna's gain, an additional measurement must be performed.

### B. Gain measurements

Gain measurements are obtained by first aligning the AUT and the MA along the maximum found in the pattern measurement. Then, different techniques can be used to find the absolute gain of the AUT. Two common methods are the gain transfer (or gain comparison) method, and the three-antenna method. An extensive description of these and other techniques can be found in [1].

The gain transfer method is based on the use of an antenna of known (standard) gain  $G_{sg}$ , whose received power, ( $P_{sg}$ ), is compared to the received power measured by the AUT, ( $P_{aut}$ ). The gain of the antenna under test, ( $G_{aut}$ ) is then found as:

$$G_{aut} = G_{sg} + P_{aut} - P_{sg}, \quad (1)$$

all quantities expressed in dB.

The three-antenna method is used when no standard gain antenna is available. In this case three antennas, all of unknown gain, are used; three measurements are taken, one for each of three combinations of transmitting and receiving antennas. For each measurement the Friis transmission equation is used and the gain of all three antennas can be found by solving a system of three equations in three unknowns, each one of the form:

$$(G_a)_{dB} + (G_b)_{dB} = 20 \log_{10} \left( \frac{4\pi R}{\lambda} \right) + 10 \log_{10} \left( \frac{P_{rb}}{P_{ta}} \right). \quad (2)$$

### C. Polarization effects

The MA can be linearly or circularly polarized. If the MA and AUT are both linearly polarized, the polarization of the AUT can be found and the co- and cross-polarization patterns can be measured. By properly mounting the MA and AUT the user can ensure that only the co- or cross-polarized pattern is measured in a 2D scan. This is not possible when performing a 3D scan; therefore, two scans must be performed, rotating the MA by 90 degrees between each scan.

If one antenna is circularly polarized and the other linearly polarized, polarization mismatch can no longer occur. However, no polarization information can be obtained, and the gain measurement obtained will be 3 dB lower than the actual value.

All these factors can lead to substantially different designs and operating procedures. In the following section the details of our approach are presented and our rationale explained.

## III. DESCRIPTION OF SYSTEM

### A. RF architecture

1) *Approach*: The design of the RF section is inspired by a main competition requirement: a system operating at

a frequency of 2.4 GHz. Many consumer devices radiate in this frequency, including Wi-Fi (IEEE 802.11 b/g) and Bluetooth (IEEE 802.15) devices, cordless phones, and microwave ovens. This results in significant interference in the 2.4 GHz band. However, this also makes a multitude of inexpensive RF devices accessible to the designer. In addition, the Wi-Fi standard provides mechanisms implemented at both the physical and data link layers to avoid collisions, reject noise, and even estimate the power of a received signal. For these reasons, our design is based on the use of two inexpensive and widely available Wi-Fi routers. One router acts as a transmitter, generating an RF signal. The other measures the received power of this signal, allowing antenna gain and pattern measurements to be made.

The IEEE 802.11 family of protocols envisions "an optional parameter that has a value of 0 through RSSI Max. This parameter is a measure by the PHY of the energy observed at the antenna [...]. RSSI is intended to be used in a relative manner. Absolute accuracy of the RSSI reading is not specified" [2]. This generic definition is implemented by manufacturers in different ways, with the goal of providing the user a visual estimation of the strength of a Wi-Fi network. The RSSI is computed by estimating the power in the preamble of a Wi-Fi beacon. An Access Point (AP) transmits this beacon repeatedly at fixed intervals, broadcasting basic information about the Wi-Fi network that the AP is creating. Devices that receive this beacon generate an estimate of the incident signal power. This mechanism allows us to obtain not only a received power estimate, but also to discriminate between different networks, and obtain a measure with improved noise immunity.

The router chosen to function as both the signal generator and received power meter is the Linksys WRT54G. This choice is motivated by two main factors. The first is that according to the manufacturer's specifications, Linksys routers provide their RSSI reading as an integer between 0 to 100. This appears to be the finest quantization of the RSSI measure offered by commercial routers, resulting in better sensitivity to small RSSI changes. The second reason is that the Linksys WRT54G supports customized firmware maintained by a large open source community. This open source firmware allows the user to manipulate otherwise inaccessible parameters, such as the transmit power and the beacon transmission interval. An SSH shell interface is also available in some versions, allowing command line control of the device. We chose the dd-wrt v24 Micro-plus firmware, which specifically allows SSH access.

2) *Calibration*: RSSI is a precise measure of the incident power, but not an accurate one. While repeated tests under the same conditions lead to repeatable results, the result cannot be used to directly measure incident power. Calibration is needed to relate RSSI to gain. To calibrate the system, the following procedure is adopted. Any antennas can be used as the MA and the AUT; neither needs to be characterized precisely. A splitter allows the signal received by the AUT to be sent to the receiving router and to a spectrum analyzer. The router RSSI and spectrum analyzer measurements are recorded for a range of transmitter power levels. The transmitted power is

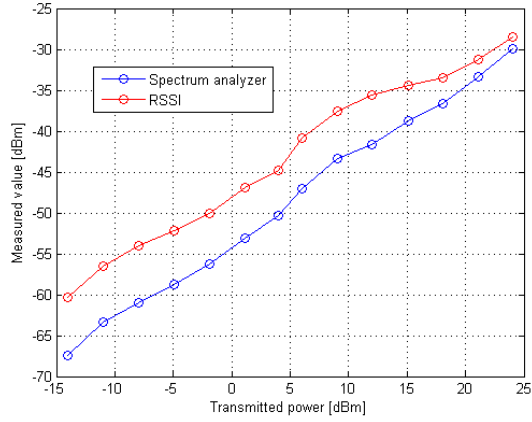


Fig. 2. Incident power on the AUT measured using RSSI and a spectrum analyzer

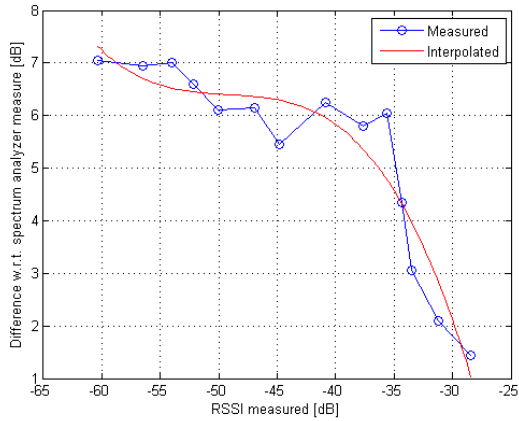


Fig. 3. Difference between the RSSI value returned by the router and the spectrum analyzer measurement as function of the RSSI itself

varied in increments of 3 dB to cover its full dynamic range. The router RSSI readings and the spectrum analyzer power measurements are shown in Fig. 2.

The nonlinearities that appear in the spectrum analyzer measurement are caused by differences between the desired transmitted power and the actual transmitted power. The RSSI is linear within an approximately 30 dB range of incident power.

The difference between the two measurements is shown in Fig. 3. It can be seen that the difference between the two readings is small for high levels of received power and increases when the signal strength decreases. The measured differences are interpolated using a third order polynomial estimator, which allows a correction coefficient to be computed from the following function:

$$C = -0.00057 * RSSI^3 - 0.0836 * RSSI^2 - 4.1314 * RSSI - 61.863. \quad (3)$$

This correction coefficient is applied to the RSSI values obtained from the router, allowing the RSSI values to match

the power measurements obtained from the spectrum analyzer.

This calibration operation is advisable, but it is not strictly necessary. Since the routers proved to behave sufficiently linearly, the RSSI reading could be used directly as a power estimate, adding only a few decibels of uncertainty in the measured result. Because the routers are mass produced, it may also be possible to assume that all routers of this model and version number will behave similarly. This would allow the same calibration to be reused.

3) *Pattern measurement*: Our LabVIEW interface allows fully automated measurement of radiation patterns in either principal plane. The user can specify which principal plane to scan, the angle to scan, and the angular separation between data points. The user can also opt to average several measurements for each data point. The computer uses the router's SSH interface to retrieve RSSI measurements and controls the driver used to rotate the positioner. Once the desired angular span is covered, the normalized pattern is displayed on a polar plot.

This procedure is valid regardless of the MA used, given that care is taken in mounting the antennas so that they are co-polarized. Nonetheless, to avoid reflections from the environment it is advisable to choose a directive antenna with a narrow main lobe. The MA should be in the far field of the AUT, with its main lobe pointed directly at the AUT.

For a 3D scan two sets of measurements are needed to avoid spurious cross-polarization effects. The MA is first mounted to produce a vertically polarized field, and both axes are scanned. Then the MA is rotated 90 degrees and the scans are repeated. The first measurement returns the theta-polarized part of the radiation pattern, while the second returns phi-polarized component. The two components can be combined together to obtain the total radiation pattern. Because the received electric field is measured only in terms of power (i.e. magnitude squared), the two sets of measurements are summed in this way:

$$G_{aut} = \sqrt{G_{\theta}^2 + G_{\phi}^2}. \quad (4)$$

4) *Gain measurement*: To obtain an absolute gain measurement we use the gain comparison technique. This method requires a standard gain antenna, but offers some advantages over the three antenna method. The three-antenna method requires knowledge of many parameters: the distance between the antennas, the transmitted power, and an accurate measure of the received power. In addition, all three antennas must be identically aligned and impedance matched, and reflections need to be minimized. Most of these variables cannot be rigorously controlled in our system. The estimated gain proved to be unreliable, with large variations between trials.

In the gain comparison method, the only parameters required are the gain of a known antenna and received power measurements obtained with the known antenna and the AUT. This implies that as long as the transmitted power and the distance between the MA and AUT are not changed, the power incident on the receiving antenna will be constant. In order to

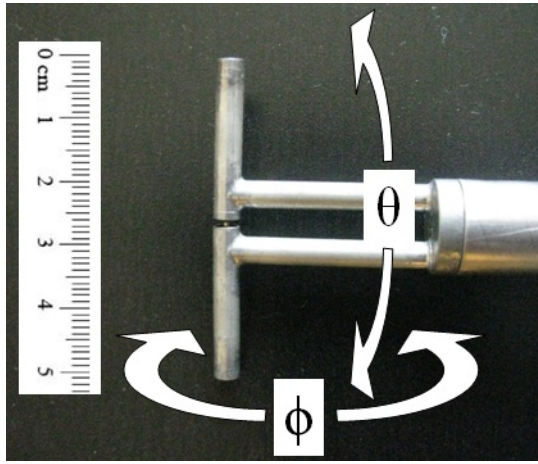


Fig. 4. 3 GHz dipole antenna

further improve the measurement, multiple RSSI readings are taken for a range of transmitter power levels and averaged. It is important to remark that the MA and the standard gain antenna serve different purposes. The MA works as a transmitter and does not need to be known, while the standard gain antenna works as a receiver and needs to have a known absolute gain.

In industry, expensive standard gain horns are normally used for gain comparison measurements. To minimize the number of antennas users need to purchase, we determined the gain of our MA. Users can then use this MA as a standard gain antenna when performing a gain measurement. Any user supplied antenna can be used as the MA during the gain measurement. To determine the gain of our MA, we performed a gain comparison measurement using a half-wave dipole. The gain of the dipole can be determined analytically to be 2.1 dBi. This antenna was available in our lab at no cost, and is only needed once to determine the gain of the MA.

5) *Antenna selection:* A planar Yagi antenna is selected to serve as the MA during pattern measurements, and as the standard gain during gain measurements. A linearly polarized antenna was chosen because linearly polarized antennas are widely available for use in Wi-Fi. The Yagi is a directive antenna, which helps minimize the effect of reflections. The gain of the Yagi is determined by performing a gain comparison measurement with a half-wave dipole, allowing it to also function as a standard gain. While the dipole offers a known gain and can be constructed easily, its low directivity would result in more reflections from the environment. Therefore, a dipole was not chosen as the MA.

To validate the system, we chose to test a 2x2 planar array of microstrip patch antennas. This antenna is also linearly polarized. Its array factor can be computed analytically, and its far field pattern can be determined through simulation. Comparing our measurements to the analytical and simulation results will allow the performance of our system to be judged.

The dipole, patch array, and Yagi antennas are shown in Fig. 4, 5, and 6 respectively. The coordinate system used to measure each antenna is also indicated.

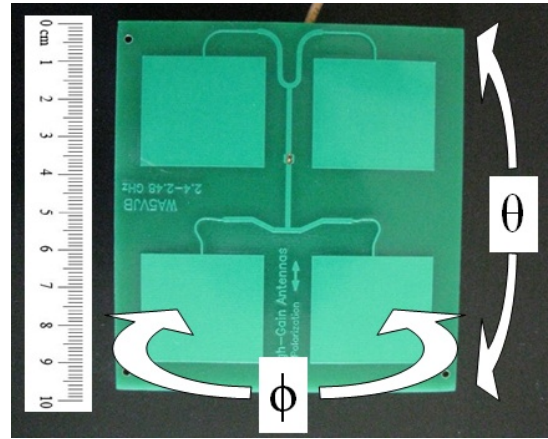


Fig. 5. 2x2 array of microstrip patch antennas

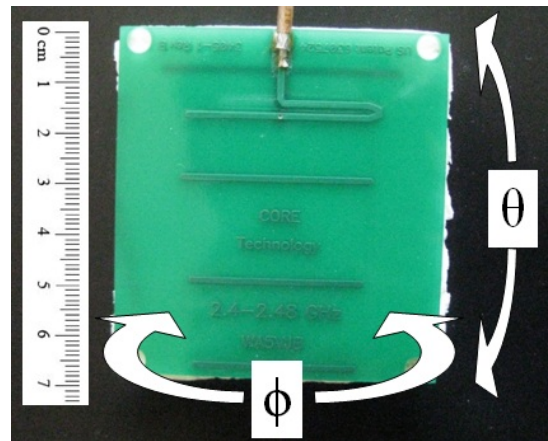


Fig. 6. 5-element Yagi antenna

### B. Two-axis positioner design and assembly

The positioner is designed with three objectives in mind. First, it must be able to rotate the AUT with the necessary precision, and provide a stable and repeatable platform for measurements. Second, it must cause minimal scattering of the incident field, so that the behavior of the AUT is not influenced by the structure. Finally, constructing the positioner needs to be within the capabilities of students who may not have extensive experience with fabrication.

We elected to use stepper motors to move the positioner. Stepper motors allow rotation in predetermined increments, so they allow the positioner to be rotated through the desired angle by simply specifying the number of steps to move. The size of each step is extremely consistent, allowing open loop control of the motors. We configured the drive to operate in microsteps, which provides the lowest level of vibration and highest control of the positioner. In this mode, each step rotates the shaft of the motor  $0.225^\circ$ . The motors are driven by a Xylotex 3-Axis Stepper Motor Driver Board. This board accepts signals from a PC parallel port, and provides the necessary outputs for driving stepper motors. The driver, motors, and power supply are available as a kit from Xylotex,

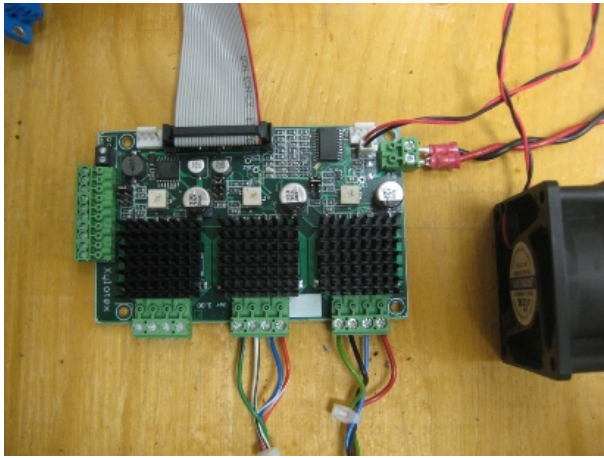


Fig. 7. Xylotex stepper motor driver board

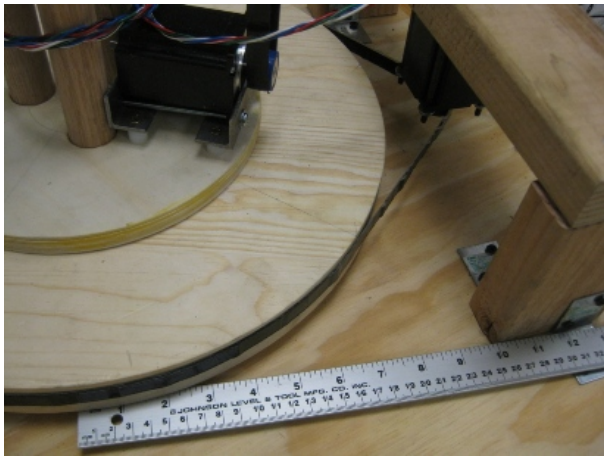


Fig. 8. Yaw axis motor, belt and pulley. The roll motor is mounted on the large yaw pulley

simplifying the design.

A stepper motor drives each axis through a belt and pulley system. While a direct drive between a wheel on the shaft of the motor and the base of the column was initially considered, this was abandoned when it was found that this would require the base to be perfectly concentric. The belt drive allows consistent, repeatable movements even if the base is not completely circular. In the yaw axis the motors operate at a gear ratio of approximately 17:1. This equates to a single step precision of  $0.013^\circ$ . To maximize accuracy, the exact gear ratio is determined empirically after the system is constructed.

The roll axis is driven by a stepper motor attached to the base of the column. This reduces the effects of scattering from the conductive body of the motor. Here the belt drive also allows increased separation between the motor and the axis. The gear ratio is approximately 6:1, resulting in a single step rotation of  $0.038^\circ$ .

The column is constructed of 1.25 in (3.18 cm) oak dowels, with the ends attached to wooden disks using mortise and tenon joints. The disks are fabricated to make this joint strong and easy to assemble. Each disk is made by laminating several



Fig. 9. Column supporting the upper disc and the roll wheel

0.125 in (0.32 cm) thick disks together. A set of three disks is laminated together, and 1.25 in (3.18 cm) holes are drilled into the disks to accept the dowels. The holes are located  $120^\circ$  apart using a geometric construction. Two more disks are then laminated onto the drilled disk, so that the finished disk has three holes that are guaranteed to be of equal depth. This process is repeated for a second disk. The dowels are then glued into each hole in the disks, resulting in a strong and square column.

The largest available 0.125 in (0.32 cm) thick disks were 10 in (25.4 cm) in diameter, which did not provide enough room to mount the roll axis motor. Therefore, the entire column was then attached to the next largest available disk, an 18 in (45.7 cm) diameter, and 1 in (2.54 cm) thick circle. This disk came with a rounded edge. To make the edge more suitable for a belt drive, the radius was removed using a band saw at the UIC machine shop. The work was performed at no cost. The disk was mounted on a 12 in (30.5 cm) diameter turntable bearing, which was then fixed to a 24 in x 24 in (61 cm x 61 cm), 0.75 in (1.90 cm) thick plywood base.

The centers of the 18 in (45.7 cm) disk and the disk at the bottom of the column were found using geometric construction. A hole was drilled in the disk at the bottom of the column, so that the center of the 18 in (45.7 cm) disk would be visible when the column was centered on the larger disk. The column was then secured to the base using wood screws.



Fig. 10. Roll axis complete with roll pulley, shaft, bearings and belt flange. The shaft is cut longitudinally to allow for easy AUT connection with, for example, double-sided tape, like shown in this figure

To allow rotation in the roll direction, an additional bearing was needed. The bearing is supported by a section of 2 in x 4 in (5.08 cm x 10.16 cm) lumber attached to the top of the column. A 1.25 in (3.18 cm) diameter hole is drilled in this bearing block to accept a bearing and a shaft to mount the antenna. The hole is located high enough to allow the antenna to roll through 360°, and is offset from the center of the column so that the antenna can be mounted on the yaw axis of rotation. To prevent scattering from a metallic bearing, a plastic sleeve bearing is selected. This bearing fits into the bearing block and is held in place by a flange. The bearing accepts a 1 in (2.54 cm) oak dowel, allowing the shaft to turn freely while being held orthogonal to the yaw axis. A pulley is fabricated from 6 in (15.24 cm) diameter, 0.125 in (0.32 cm) thick disks, and secured to the dowel using a plastic shaft collar. A plastic shaft collar with mounting holes on its face was not available, so holes are drilled through the collar and the pulley so that nylon machine screws can be used to attach the pulley to the shaft.

Obtaining pre-made belts in the correct sizes also proved difficult, so we chose to fabricate our own belts. The belts are constructed out of several layers of adhesive tape. To construct the belts, the required circumference is measured. Then the pulleys are clamped to a table to provide a stable surface. The distance between the pulleys determines the circumference of the belt. To provide durability and a high friction interface between the belt and pulleys, the inner surface of the belt is made of duct tape. Several layers of Scotch brand transparent tape are then applied over the duct tape, followed by a final outer layer of duct tape. This method produces an inexpensive and resilient belt in any length desired.

The roll axis motor must rotate with the column when it is moved around the yaw axis, so it is mounted to the base of the column. We fabricated our own mount from a 0.125 in (0.32 cm) thick 1 in x 1 in (2.54 cm x 2.54 cm) angle iron profile. First, we cut two 3.5 in (8.89 cm) long segments from the profile. Using a #5 (0.522 cm) drill bit, we then drilled holes in each segment to match the mounting holes on the

face of the motor. On the other side of the profile, we drilled and countersunk holes for wood screws. The two profiles are attached to the motors using long #10 (0.483 cm) machine screws and nuts, which are then cut to length. Nylon spacers are placed underneath the mount so that the height of the motor can be adjusted if necessary. This allows the tension in the belt to be altered. Wood screws secure the motor to the base of the column. To enhance friction between the motor and the belt, a 1 in (2.54 cm) soft rubber wheel is used as the drive pulley for the motor.

The yaw axis motor is suspended upside down to allow its shaft to be in the same plane as the base of the column. A brace is constructed of 2 in x 4 in (5.08 cm x 10.16 cm) lumber, held together by wood screws. Slots are cut in the top of the brace so that the position of the motor can be adjusted if necessary, as when installing or removing the belt. Long #10 (0.483 cm) machine screws between the mounting holes of the motor and the slots in the brace secure the motor. A 1 in (2.54 cm) soft rubber drive wheel is used as a pulley here as well. The brace is secured to the plywood base plate using right angle joist brackets.

In addition to the positioner, we also needed to hold the MA in a fixed position. The base of the MA mount is an 18 in x 18 in (45.72 cm x 45.72 cm) square cut from a 3/4 in (1.90 cm) thick sheet of plywood. Self-adhesive felt feet are placed under the base to improve its stability. A 36 in (91.44 cm) long segment of 2 in x 4 in (5.08 cm x 10.16 cm) lumber is oriented vertically above the center of the base. Right angle joist brackets are used to ensure that the vertical segment is normal to the base, and wood screws are used to secure it to the base. The mount is tall enough so that the height of the MA can be adjusted so that it is aligned with the AUT. The mount is suitable for attaching several antenna geometries. The mounting procedure is similar to that used with the AUT. Styrofoam blocks are placed between the mount and the antenna to prevent anomalies caused by locating microstrip lines next to dielectric materials other than air. The antenna is secured using double-sided tape. Other antennas, such as the dipole, can be secured using nylon cable ties.

### C. Software

A LabVIEW application is developed to control the movement of the positioner and to retrieve the RSSI measurements from the router. LabVIEW makes it easy to develop a sophisticated GUI and a hardware interface suitable for motor control.

The positioner's motions are controlled using the computer's parallel port. The mapping of the data register of the parallel port is shown in Table I.

The LabVIEW program determines the direction and amount of rotation, and computes the number of micro-steps necessary. It then applies the appropriate values to the parallel port. The direction of rotation is controlled by the direction bit, and the motor rotates one microstep each time a rising edge occurs on the step bit. The same procedure is valid for both axes.

TABLE I  
PARALLEL PORT DATA REGISTER BITS

Bit #	Function
0	Direction axis 1
1	Stepping axis 1
2	Direction axis 1
3	Stepping axis 2

The program Plink is used to communicate with the router. Plink is a freeware tool that provides a Windows-compatible SSH client. Combined with the dd-wrt firmware, it allows an SSH connection to be established automatically. LabVIEW executes Plink, opens an SSH connection and authenticates itself as *root* user, executes the command `wl -rssi`, and reads the standard output of Plink to retrieve the RSSI measure. The procedure is completely automated and requires no user intervention.

The program allows the user to rotate the axes and take measurements manually, or to run automated scans of the principal planes. To perform an automated scan, LabVIEW executes a series of movements, each followed by an RSSI measure. The span, angular step size and axis to control are defined by the user, as is the number of RSSI samples to collect and average for each position. The program uses the interpolator polynomial described in the RF architecture section to automatically determine the correction to be applied. When the scan is completed the data collected are saved as an ASCII text file and presented to the user in the form of a polar plot. During the scan operation no user intervention is required at all.

The speed of a scan is determined by the amount of movement requested, by the step size, and by the number of samples to average. A 360-degree scan with steps of 5 degrees and 8 RSSI samples per position takes approximately 20 minutes. By combining multiple scans for different AUT positions in an environment such as MATLAB, full 3D patterns can be obtained from the raw ASCII text files saved by LabVIEW. For the purpose of demonstrating the operation and capabilities of the system, only 2D cuts are presented in the Test Results section.

#### IV. BILL OF MATERIALS

Description	Source	Cost (\$)
<b>RF Measurement</b>		
Linksys WRT54G, 2x	Amazon	113.08
Ethernet cable, 10 ft	Amazon	3.95
PCB Patch Antenna	Amazon	34.95
PCB Yagi Antenna	Amazon	32.95
RP-TNC / N-m, 2x	Amazon	9.96
Adpt N-f / SMA, 2x	Amazon	8.26
Adpt SMA-f / SMA-f, 2x	Digikey	8.90
SMA cables, 4 ft, 2x	L-com.com	36.00
<b>Software</b>		
LabVIEW student license	NI.com	59.95

<b>Positioner control</b>		
Motor kit	xylotex.com	310.00
DB25 10 ft extension	Amazon	3.99
Braided wire	Home Depot	5.00
<b>Positioner hardware</b>		
Plywood base	Home Depot	7.00
18 in Wood Circle	Lowe's	13.17
12 pk 10 in Wood Circle	craftparts.com	11.88
6 in Wood Circle, 12x	craftparts.com	7.44
1 1/4 in x 36 in Dowel, 3x	craftparts.com	18.75
12 in Turntable	McMaster	10.67
8 ft 2 in x 4 in Lumber	Home Depot	1.98
1in x 36in Oak Dowel	Home Depot	4.37
Acetal Flanged Bearing	McMaster	9.60
Slimline Drive Roller, 2x	McMaster	59.36
Transparent Tape, 1/2 in	Staples	7.49
Duct Tape, black	Staples	7.99
1 in x 1 in Angle Iron	Home Depot	7.10
Clamp on Shaft Collar	McMaster	14.39
Nylon Screws 2in	McMaster	7.23
Nylon Hex Nuts, 3/8in	McMaster	6.24
Plastic Mesh Flange	Joann fabric	0.60
Tension Pins, Spacers	Home Depot	15.16
Machine Screws and Nuts	McMaster	27.05
Screws, Joist Angles, Glue	Menard's	16.01
Carpet Tape	Ace Hardware	4.92
12 3/4in Felt Pads	Home Depot	3.61
Shipping costs, total		35.46
<b>TOTAL</b>		<b>924.46</b>

#### V. TEST RESULTS

The performance of the system was evaluated by measuring the far field patterns of the patch array, dipole, and Yagi antennas. The test was performed outdoors to minimize the effect of reflections, in the area behind a team member's home. The test setup is shown in Fig. 11. The test area was approximately 5 m x 5 m square, with the main lobe of the MA pointed at a wooden fence. The positioner and MA were placed on tables to elevate them above the ground. The ground consisted of a grass lawn and a concrete surface. The positioner was placed over the grass region, as we felt this would minimize the effect of scattering on the measurement. The relative permittivity of soil,  $\epsilon_r$ , is approximately 3, compared to 4.5 for concrete. As will be shown below, the ground was the largest source of reflections. A 360° scan in 5° increments was made in both principal planes of each antenna. Eight samples were averaged in each position.

To validate the test results, the far fields of the patch array, Yagi and dipole antenna were simulated using FEKO. The curved microstrip feed structure of the patch array proved difficult to replicate in FEKO. Therefore, we simulated each patch with its own feed, with all the patches feed in phase and with the same amplitude. The patch is also simulated with an infinite substrate. This provides a reasonable approximation of the far field pattern of the patch array. The measured values



Fig. 11. Outdoor measurement setup

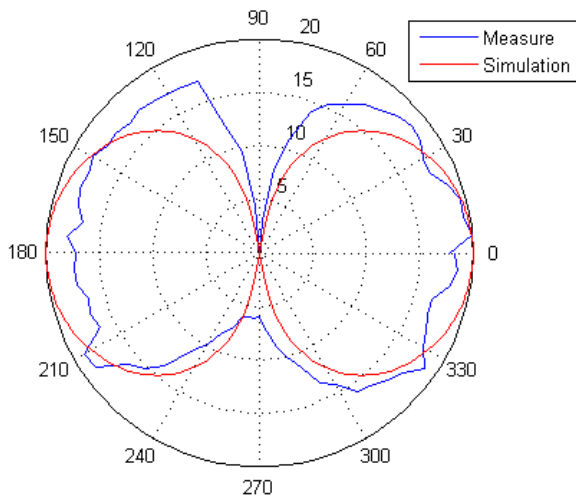


Fig. 12. Dipole antenna,  $\theta$  principal plane

are normalized, and superimposed with the simulation results to facilitate comparison.

#### A. Half-wave dipole

The pattern of the dipole is well known and can be determined analytically with relative ease. Because of this, measuring a dipole will provide an excellent example of the performance of our system. In the  $\theta$  plane, the half-wave dipole is expected to have a toroidal pattern. Our measured results clearly show this toroidal pattern, with nulls at  $90^\circ$  and  $270^\circ$ . Both the simulated pattern and the measured pattern are shown in Fig. 12. While some irregularities are present, the distinct pattern of the dipole is readily apparent.

In the  $\phi$  plane, the half-wave dipole is expected to have a perfectly circular pattern. The measured result and simulation results are shown in Fig. 13. Some irregularities between measured and simulated data are expected, and the measured results do not show an extreme deviation from the expected circular pattern. By comparing our test results to the well

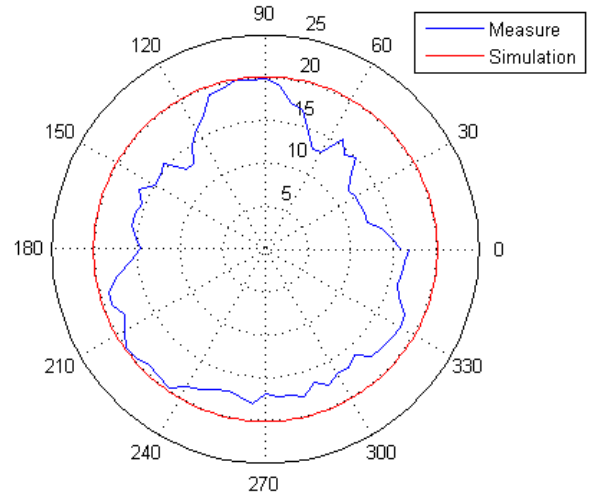


Fig. 13. Dipole antenna,  $\phi$  principal plane

defined pattern of the half-wave dipole, we can conclude that our system provides reliable pattern measurements.

#### B. 2x2 patch array

Based on the simulation results, the patch array is expected to produce a single, large lobe. This is confirmed by an analytical computation of the array factor of a 2 by 2 planar array. Because the simulation is performed with an infinite substrate, the actual results will show some variation due to diffraction effects from the finite substrate. The measured results in the  $\theta$  plane are shown in Fig. 14 along with the simulation results. The measured results clearly show a single large lobe, with a small back lobe. Small side lobes are also present; these may be the results of the finite substrate of the array. Due to the symmetry and recurrence of these features in multiple measurements, we do not believe they are spurious. They are also visible in the  $\phi$  plane, as seen in Fig. 15. The large main lobe in the  $\phi$  plane coincides well with the simulation results, and the small side lobes are present here as well, further proof that they are legitimate.

While conducting the measurements of the patch array, we were able to observe the effect of reflections off the ground. These were first recognized as distinctive asymmetrical lobes in the  $\theta$  plane pattern of the array. These lobes occurred when the broadside lobe and the backlobe were pointed towards the ground. Comparing Fig. 16 (left) with Fig. 14, the large lobes at  $300^\circ$  and  $145^\circ$  are very noticeable.

To confirm that this effect was due to reflections off the ground, the scan was repeated while rotating the positioner in the opposite direction. Because the  $0^\circ$  position is always assigned to the start of the scan, with the angle increasing as the scan progresses, the pattern should be reflected by  $180^\circ$ . This is indeed the case, as is shown by Fig. 16 (right). In this case the main lobe is pointed at the ground at  $60^\circ$ , and the back lobe is pointed at the ground at  $225^\circ$ . Fig. 16 (right) is a near perfect reflection of Fig. 16 (left).

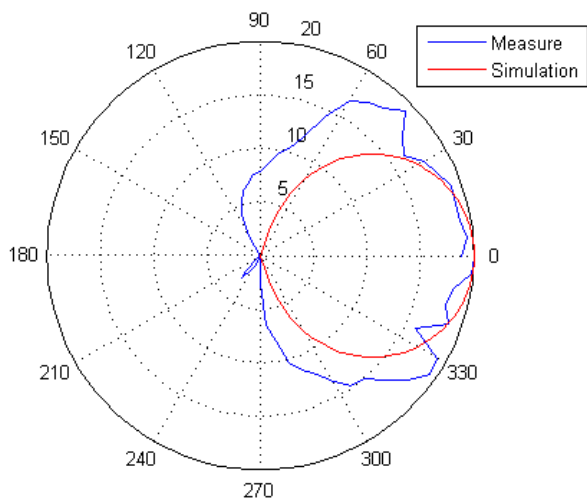


Fig. 14. Patch array antenna,  $\theta$  principal plane

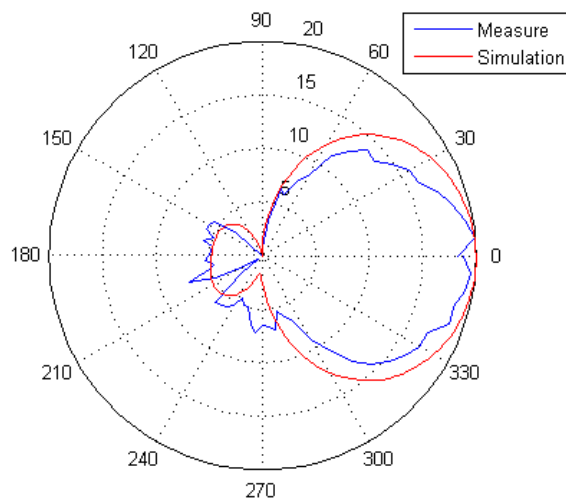


Fig. 17. Yagi antenna,  $\theta$  principal plane

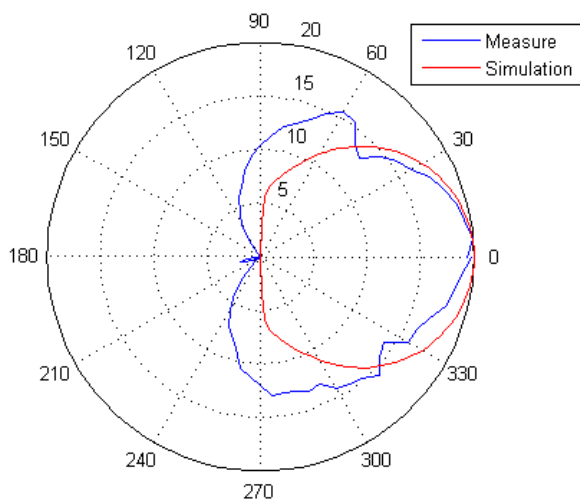


Fig. 15. Patch array antenna,  $\phi$  principal plane

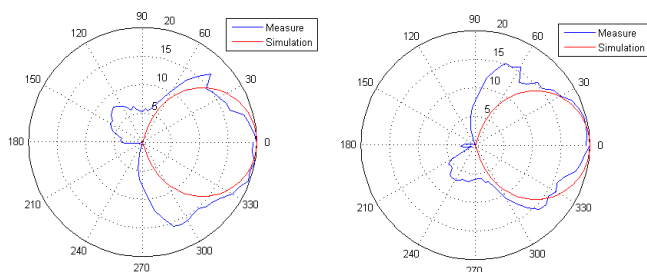


Fig. 16. Patch array antenna,  $\theta$  principal plane scanned clockwise (left) and counter-clockwise (right) showing reflection of side lobe positions

The surface of the ground was wet from recent rain, which likely increased the relative permittivity of the surface and increased its reflection coefficient. To eliminate this effect, we performed the scan again, this time scanning with the yaw axis of the positioner. To maintain the co-polarization with the MA,

both the AUT and the MA were rotated. In this configuration, the AUT is never pointed at the ground. Fig. 14 shows that the ground reflections are no longer present when this method is used. Unless otherwise indicated, all results shown here were gathered using yaw scans. This effect may be diminished when the surface is dry, however, this test condition was difficult to obtain at our locale.

### C. 5-element Yagi

Unlike the dipole and the patch array, an analytical computation cannot be made to confirm the simulation results of the Yagi antenna. However, our previous measurements have been very representative of the results obtained analytically and through simulation. We show that the measured pattern of the Yagi antenna also represents the expected pattern accurately. The entire Yagi antenna is simulated, including the feed structure, on a finite dielectric substrate. In the  $\theta$  principal plane, a large main lobe is expected, along with a smaller back lobe. The measured results in Fig. 17 show a large main lobe that coincides very well with the simulation results. A small additional back lobe is present. This may be the result of scattering caused by the coaxial feed cable mounted on the back of the antenna.

### D. Gain

The gain measurement procedure is tested on the 5-element Yagi, which is advertised as having an 8.5 dBi gain, and on the patch array, which is advertised as having an 11.5 dBi gain. A half-wave dipole available in the lab is used as the standard gain antenna. A half-wave dipole is expected have a gain of 2.15 dBi. However, the dipole at hand was designed to operate at 3 GHz, making it slightly smaller than a half-wave length at 2.4 GHz. Therefore, we estimate the gain at 2.4 GHz to be 2 dBi. Once the gain of the Yagi antenna is known, the half-wave dipole is not needed. The Yagi itself can be used as the standard gain antenna for future gain measurements. When performing a gain measurement any antenna can be used as

TABLE II  
GAIN MEASUREMENT TEST, YAGI ANTENNA

$P_t$ [mW]	$G_{sg}$ [dBi]	$P_{sg}$ [dBm]	$P_{aut}$ [dBm]	$G_{aut}$ [dBi]
128	2	-41.0	-35.0	8.0
64	2	-44.9	-38.9	8.0
32	2	-49.0	-39.9	11.1
16	2	-50.5	-41.4	11.1
8	2	-53.6	-44.9	10.7
			<b>Average</b>	<b>9.8</b>

TABLE III  
GAIN MEASUREMENT TEST, PATCH ARRAY

$P_t$ [mW]	$G_{sg}$ [dBi]	$P_{sg}$ [dBm]	$P_{aut}$ [dBm]	$G_{aut}$ [dBi]
128	2	-43.6	-37.6	7.9
64	2	-49.1	-39.1	12.0
32	2	-51.5	-41.9	11.6
16	2	-53.9	-44.3	11.6
8	2	-56.3	-48.3	10.0
			<b>Average</b>	<b>10.6</b>

the MA. When measuring the gain of the Yagi in our tests the patch array was used as the MA. The Yagi was used as the MA when measuring the gain of the patch array. The gain measurements of the Yagi are available in Table II.

The gain measurements of the patch array are presented in Table III. The Yagi antenna shows a larger discrepancy from its nominal value (1.3 dBi difference) than the patch array (0.9 dBi difference). It is not known how the manufacturer determines the gain of these antennas, or what tolerance is expected in the nominal gain. Additional errors may be introduced by mechanical misalignment of the antennas, imperfect impedance matching, and by operating in a non-anechoic environment. In particular, the Yagi antenna's reflection coefficient  $S_{11}$  proved to be very susceptible to perturbations in its near field. Even placing styrofoam in contact with the antenna's microstrip had a significant effect on the return loss. These near field effects may have contributed to the discrepancy in the gain measurement. However, as the manufacturer provides only the nominal gain, more information would be needed to adequately judge our gain measurements.

For these reasons, we believe that the goal of  $\pm 0.5$  dB error in the gain measure can be achieved in an anechoic environment, provided that particular care is taken to attach the antennas to the positioner without influencing the reactive near field of the antenna.

## VI. CONCLUSION

We have shown that it is possible to realize a complete antenna measurement system operating at 2.4 GHz using only inexpensive and readily available equipment. The designed system is able to measure accurate radiation patterns even in non-anechoic environments. Precaution should be taken in choosing the axes of rotation so as to avoid obvious reflections from surfaces such as the floor or walls, depending on the operating environment. Radiation patterns in each principal plane can be measured automatically. In principle both 2D and 3D radiation patterns can be measured, although the time required for a complete  $4\pi$  srad scan may be large.

The gain measure proved to be more difficult because of the large number of variables involved that need to be controlled. By minimizing user errors such as polarization mismatch, a reasonable argument is presented that the system could achieve  $\pm 0.5$  dB gain accuracy in an anechoic environment.

## ACKNOWLEDGMENT

The authors would like to thank Prof. Konrad Kaczmarski of UIC for his numerous design suggestions, Tadahiro Negishi of UIC for the invaluable help in simulating antennas with FEKO, and Prof. Danilo Erricolo of UIC for his guidance throughout the project.

## REFERENCES

- [1] *IEEE Standard Test Procedures for Antennas*, IEEE Std 149-1979, Published by IEEE, Inc., 1979
- [2] *IEEE Standard for Information technology. Local and metropolitan area networks - Specific requirements. Part 11: Wireless LAN Medium Access control and Physical Layer Specifications*, section 14.2.3.2, IEEE Std 802.11-2007, 2007
- [3] C. A. Balanis, *Antenna Theory Analysis and Design*, 3rd ed., Wiley-Interscience, 2005
- [4] R. H. Bishop, *LabVIEW 8 Student Edition*, 1st ed., Pearson Education, 2007
- [5] K. J. Kaczmarski, *An "exact" inverse source reconstruction*, Ph.D. dissertation, University of Illinois at Chicago, Chicago, IL, 2008



**Vittorio Picco** (S '09) was born in Mondovì (Cuneo), Italy, in 1985. He received the B.Sc. in electronic engineering and the M.Sc. (*summa cum laude*) in telecommunications engineering from the Politecnico di Torino, Italy, in 2007 and 2010, respectively. He received the M.Sc. in electrical and computer engineering from the University of Illinois at Chicago (UIC) in 2010.

Since January 2010 he is pursuing his Ph.D. degree in electrical and computer engineering at UIC, in the Andrew Electromagnetics Laboratory. His research interests include electromagnetic propagation and scattering with applications to narrowband non-destructive underground imaging, and antenna design.

Mr. Picco is a member of Eta Kappa Nu.



**Keith Martin** (S '11) was born in St. Charles, Illinois, in 1985. He received the B.S. in electrical engineering from Northwestern University, Evanston, Illinois, in 2007.

He has worked as an Electronic Engineer at PEC Products and a Systems Integration and Technology Analyst at Accenture. Since August 2011 he is pursuing his M.S. degree in electrical and computer engineering at UIC, in the Andrew Electromagnetics Laboratory. His research interests include guided and free space electromagnetic propagation and the use of computational methods.

Mr. Martin is a member of Eta Kappa Nu.